Electronic Supplementary Material (ESI) for Nanoscale.


# Supporting Information

## High Piezo-Resistive Performances of an Anisotropic Composite Realized by Embedding rGO-based Chitosan Aerogel in Open Cell Polyurethane Foams

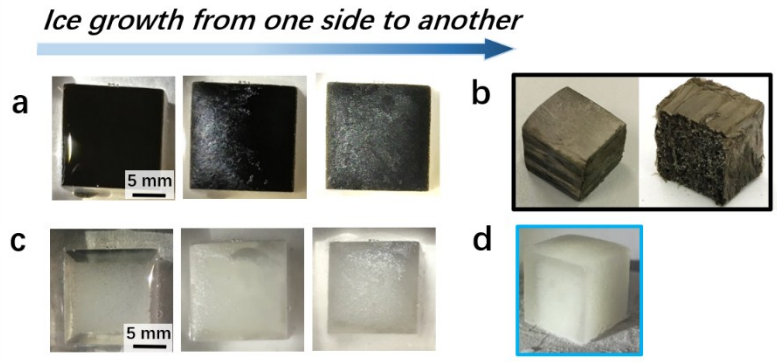


**Figure S1.** Digital photos showing the bidirectional freezing process of (a) PUF in the dark brown GO/CS solution, and (c) PUF in the transparent CS solution. (b) The resulting aerogel/PUF composites after lyophilization. (d) Digital photo of the frozen CS solution containing the PUF.

The bidirectional freezing process of the aerogel/PUF composites in the actual experiment is shown in Figure S1 (a). The ice crystals of the dark brown GO/CS solution gradually grew from left to right side until the whole solution was frozen (the arrow in the Figure shows the freezing direction and the temporal evolution). The aerogel/PUF composite was obtained after the lyophilization step. The PUF porous structure is obtained after removing the skin layer of aerogel, Figure S1 (b). Due to the fact that the GO/CS was a dark and non-transparent solution, the freezing process of the PUF frozen in the transparent CS solution has been also shown in Figure S1 (c). It can be clearly seen that all the pores of the PUF were totally filled by the solution. After freezing, the PUF can be found completely intact in the frozen CS solution (Figure S1 (d)).

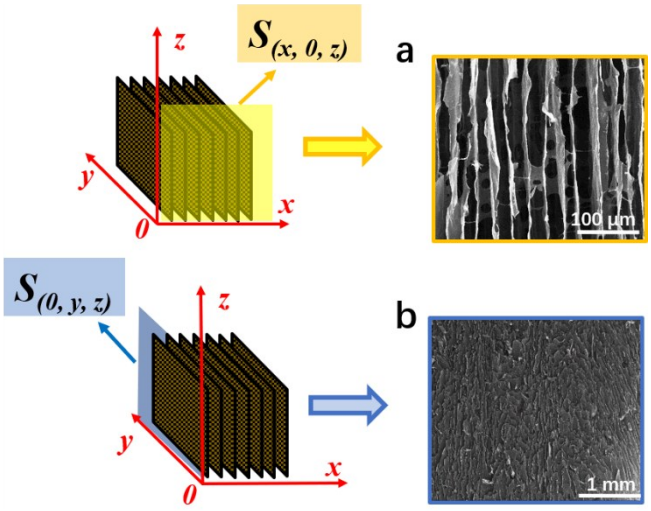


**Figure S2.** SEM images of the rGO/CS aerogel observed at (a) $S_{(x, 0, z)}$, (b) $S_{(0, y, z)}$.

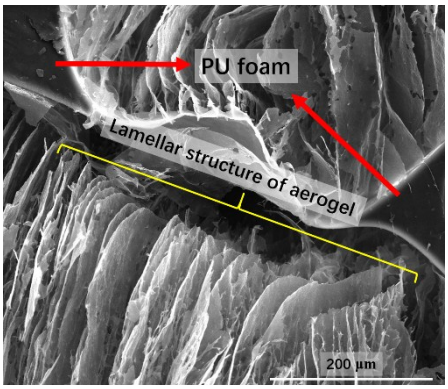


Figure S3. SEM images of aerogel/PUF composites to show the parallel lamellar structure of the rGO/CS aerogel within the polyurethane foams.

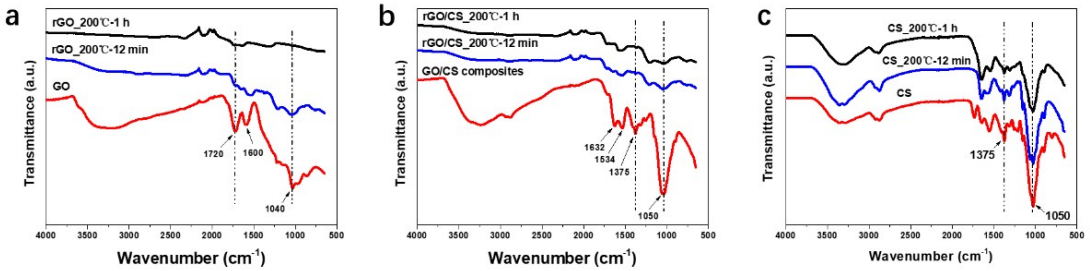


**Figure S4**. FTIR spectra of (a) GO before thermal annealing, rGO powder after annealing at 200°C for 12 min and 1h, (b) GO/CS aerogel before thermal annealing, rGO/CS aerogel annealed at 200°C for 12 min and 1h, (c) CS aerogel before thermal annealing and annealed at 200°C for 12 min and 1h.

In the spectra of GO and rGO, reported in Figure S4(a), the two characteristic bands centered at 1720 $cm^{-1}$ and 1040 $cm^{-1}$ are assigned respectively to the stretching of carbonyl group (C=O)

and C-O bond from epoxy and hydroxyl groups.[1] The absorbance intensity of both peaks significantly reduces in the sample treated for 12 min and 1 h at 200°C, as confirmation of the effectiveness of the thermal reduction. In the spectra of pristine CS and rGO/CS composite shown in Figure S4 (b), strong peaks ascribed to CS are observed at 1632 and 1534 $cm^{-1}$, corresponding to the C=O stretching vibration of –NHC(O)- and the N-H bending of $–NH_2$, respectively.[1, 2] After the thermal treatment, the absorbance intensity of the peaks at 1375 $cm^{-1}$ (C–OH) and 1050 $cm^{-1}$ (C-O) for the rGO/CS composite reduces and the peaks become difficult to be detected. This confirms that the oxygen-based groups present on surface and edges of GO platelets are completely removed during the annealing process and that chitosan has a beneficial effect on enhancing the extent of thermal reduction as compared to the thermal reduction of pristine GO.

For sake of comparison, the spectra of pristine CS annealed at 200°C for 12 min and 1 h are shown in Figure S4 (c). No apparent change can be found in the absorbance intensity of the peaks at 1375 $cm^{-1}$ (C–OH) and 1050 $cm^{-1}$ (C-O) after the thermal annealing.

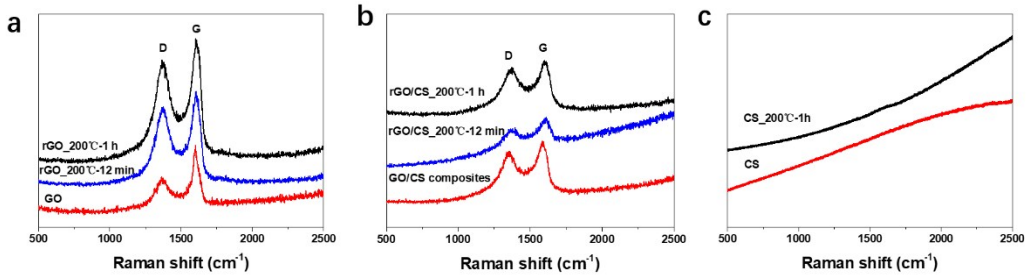


**Figure S5.** Raman spectra of (a) GO before thermal annealing, rGO powder annealed at 200°C for 12 min and 1h, (b) GO/CS aerogel before thermal annealing, rGO/CS aerogel annealed at 200°C for 12 min and 1h, (c) CS powder before thermal annealing and annealed at 200°C for 1h.

Figure S5 (a) shows the Raman spectra of GO and rGO collected after the thermal treatment, with a clear evidence of the D and G bands ascribed to surface defects and the in-plane vibration of $sp^2$ carbon atoms, respectively.[3] As for the GO sample, the ratio of intensity of D to G band ($I_D/I_G$) is a measure of disordered carbon, expressed as the $sp^3/sp^2$ carbon ratio.[4] However the Raman $I_D/I_G$ ratio provides also an estimation of the $sp^2$ domain size.[5] In this view, the increment of the $I_D/I_G$ ratio for the samples submitted to the thermal treatment is actually attributed to the increase of the amount of small in-plane $sp^2$ domains. In fact, the $I_D/I_G$ ratio for the GO powder and rGO powders obtained after thermal annealing for 12 min and 1 h at 200°C is 0.61, 0.85 and 0.87, respectively.[5, 6] However, the $I_D/I_G$ ratio measured both for the GO/CS aerogel and rGO/CS aerogel obtained after annealing for 12 min and 1 h at 200°C is 0.86, 0.84 and 0.89, respectively. Clearly, in presence of chitosan, the $I_D/I_G$ ratio trend does not show a clear increment despite no characteristic peak appears in the Raman spectra of pristine CS and CS with 1 h annealing at 200°C (Figure S5(b) and Figure S5(c)).

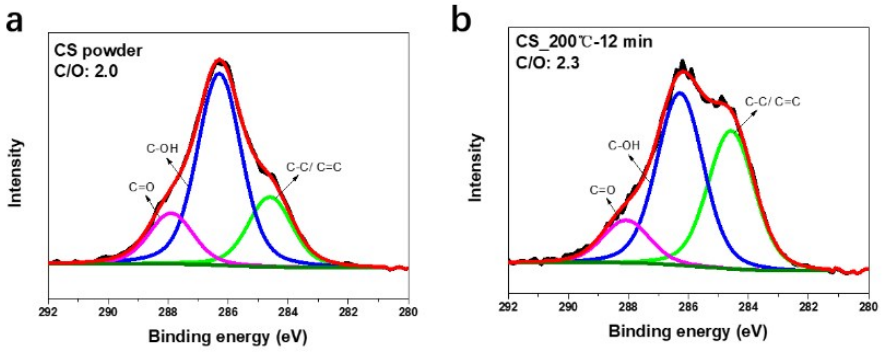


**Figure S6.** Deconvoluted $C_{1s}$ XPS spectra of (a) CS powder, and (b) CS powder annealed at 200°C for 12 min.

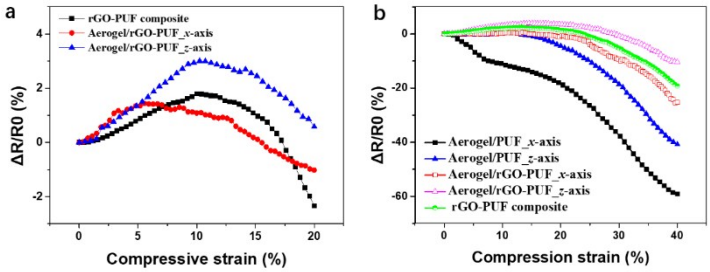


**Figure S7** (a) Normalized change of resistance ($\Delta R/R_0$) of rGO-PUF composite and aerogel/rGO-PUF composite as a function of compressive strain under 20% strain. (b) Normalized change of resistance ($\Delta R/R_0$) of rGO-PUF composite, aerogel/PUF composite and aerogel/rGO-PUF composite as a function of compressive strain under 40% strain.

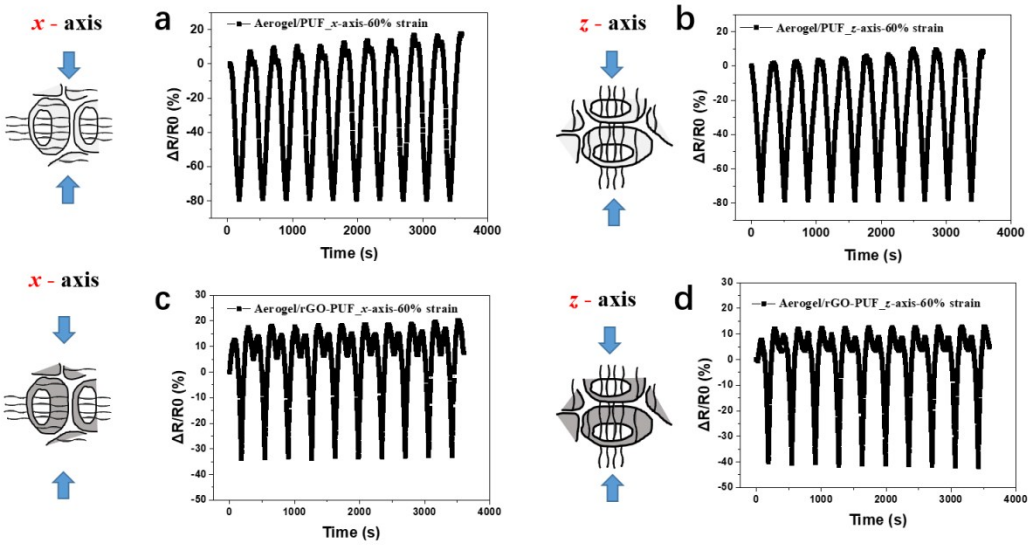


**Figure S8**. Normalized change of resistance ($\Delta R/R_0$) of aerogel/PUF composite compressed along (a) x-axis and (b) z-axis directions and aerogel/rGO-PUF composite compressed along (c) x-axis and (d) z-axis directions as a function of compressive strain under 60% strain.

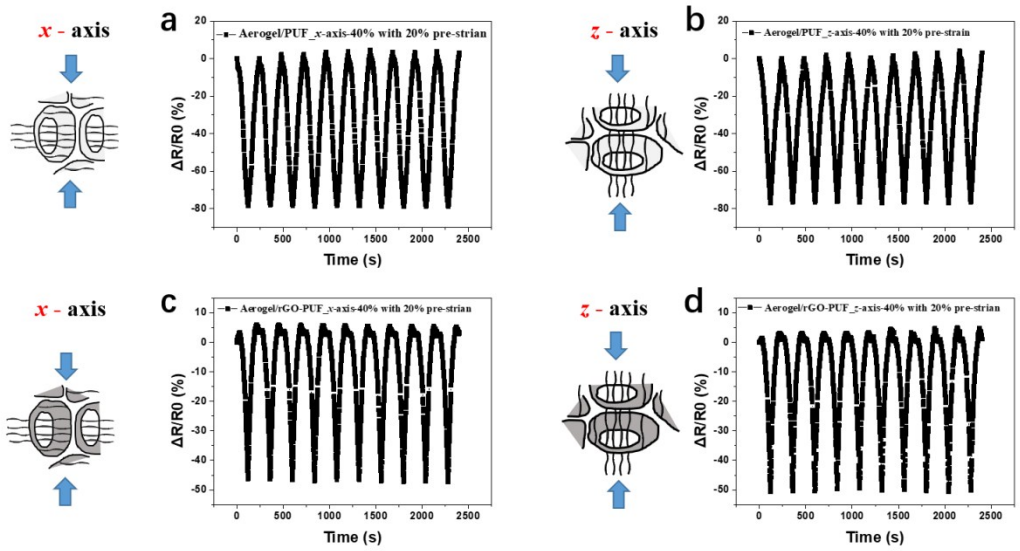


**Figure S9** Electrical resistance variations recorded in ten loading/unloading cycles of aerogel/PUF composite compressed along (a) x-axis and (b) z-axis directions and aerogel/rGO-PUF composite compressed along (c) x-axis and (d) z-axis directions under 40%strain with 20% pre-strain.

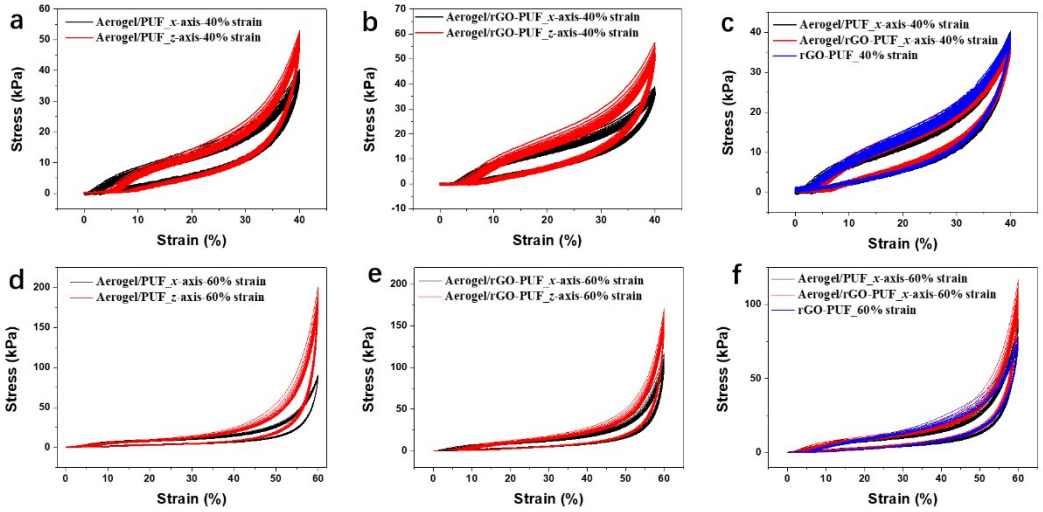


**Figure S10.** Cyclic compressive stress-strain curves for (a) aerogel/PUF composite, (b) aerogel/rGO-PUF composite and (c) all three composites compressed along x-axis direction under 40% compressive strain. Cyclic compressive stress-strain curves for (a) aerogel/PUF composite, (b) aerogel/rGO-PUF composite and (c) all three composites compressed along x-axis direction under 60% compressive strain.

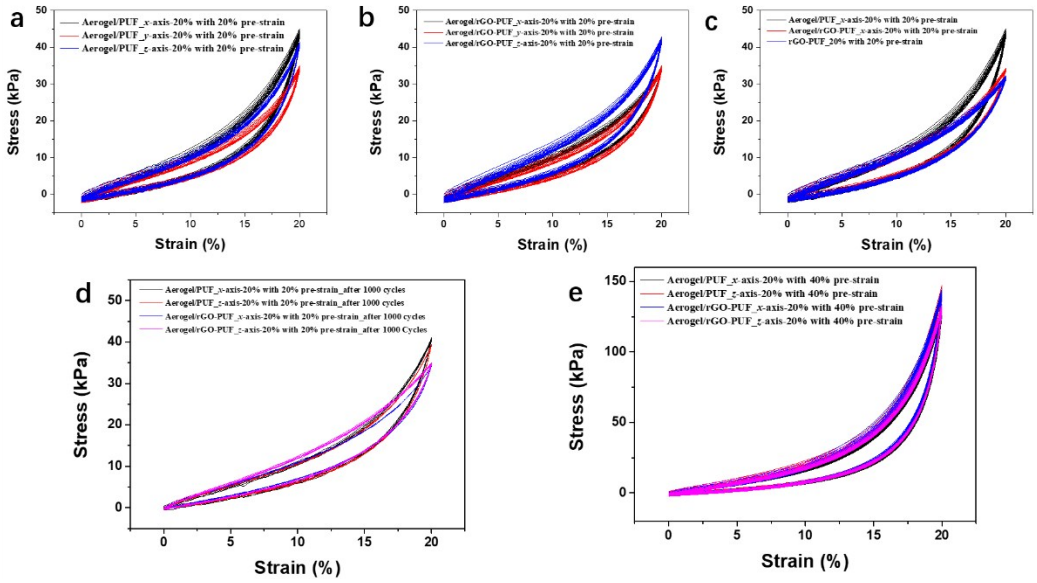


**Figure S11.** Cyclic compressive stress-strain curves for (a) aerogel/PUF composite, (b) aerogel/rGO-PUF composite and (c) all three composites compressed along x-axis direction under 20% compressive strain with 20% pre-strain. (d) Cyclic compressive stress-strain curves for aerogel/PUF composite and aerogel/rGO-PUF composite under 20% compressive strain with 20% pre-strain after 1000 compressive cycles. (e) Cyclic compressive stress-strain curves for aerogel/PUF composite and aerogel/rGO-PUF composite under 20% compressive strain with 40% pre-strain.

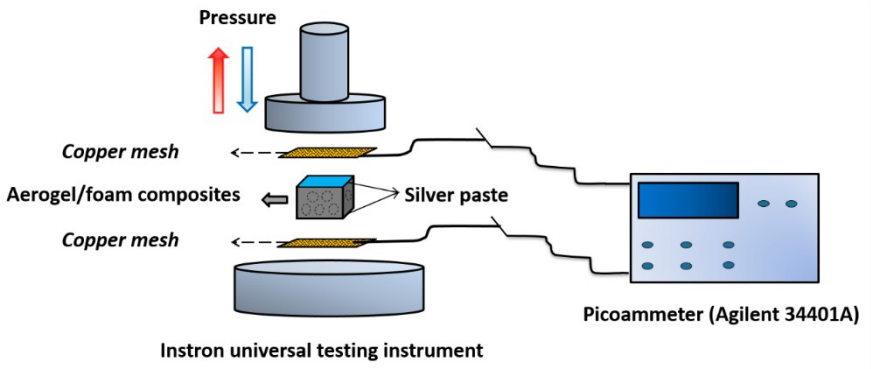


**Figure S12.** Schematic illustration of the experimental set-up for measuring piezoresistive properties of the aerogel/foam composites.

The copper mesh is used here for the purpose of enhancing the bonding strength to the sample surface, since it provides a large contact area which ensures a stable and robust bonding when sealed with silver paste.

**References**


[1] X. M. Feng, X. Wang, W. Y. Xing, B. Yu, L. Song, Y. Hu, Industrial & Engineering Chemistry Research 2013, 52, 12906.

[2] M. Lavorgna, F. Piscitelli, P. Mangiacapra, G. G. Buonocore, Carbohyd Polym 2010, 82, 291.

[3] M. S. Dresselhaus, A. Jorio, M. Hofmann, G. Dresselhaus, R. Saito, Nano Lett 2010, 10, 751.

[4] A. C. Ferrari, J. Robertson, Phys Rev B 2000, 61, 14095.

[5] S. F. Pei, H. M. Cheng, Carbon 2012, 50, 3210.

[6] M. Fang, L. A. Long, W. F. Zhao, L. W. Wang, G. H. Chen, Langmuir 2010, 26, 16771.